Extended Siponimod Release Via Low-Porosity PLGA Fibres: A Comprehensive Three-Month In Vitro Evaluation for Neovascular Ocular Diseases

Supplementary data

Rasha A. Alshaikh [a,b], Krishnakumar Chullipalliyalil [c], Christian Waeber [a,d], Katie B. Ryan [a,e]

[a] School of Pharmacy, University College Cork, Cork, Ireland.

[b] Department of Pharmaceutical Technology, Faculty of Pharmacy, Tanta University, Tanta, Egypt.

[d] Department of Pharmacology and Therapeutics, School of Medicine, University College Cork, Cork, Ireland

[c] Centre for Advanced Photonics & Process Analysis, Munster Technological University Cork, T12 P928 Cork, Ireland

[e] SSPC The SFI Research Centre for Pharmaceuticals, School of Pharmacy, University College Cork, Cork, Ireland.

S1. Supplementary methods

S1.1. Raman spectroscopy

Table S1. List of the parameters used for the solid-state characterisation of unprocessed and electrospun samples with Raman spectroscopy.

Acquisition Parameter	Z depth mapping	Distribution Mapping (High resolution)	Single spot acquisition
Acquisition time (s)	60	25	30
Accumulations	1	1	1
Grating (gr/mm)	600	600	600
Power	30 mW	30 mW	30 mW
Objective	×100	×50 ×100	×50
Points per Line, X-axis	NA	5	NA
Lines per Image, Y-axis	NA	10	NA
Layers in Stack/No of points Z axis	50	3	NA
Scan Width [µm]	NA	4.000	NA
Scan Height [µm]	NA	11.800	NA
Stack Depth [µm]	10	3.500	NA
Data Range (cm^{-1})	From:1400 To:1700	From:1400 To:1700	From: 250 To: 3000

S1.2. Thermogravimetric analysis (TGA)

All samples were analysed using a thermogravimetric analyser TGA Q500 (TA Instruments, New Castle, DE, USA). Samples of known weight (6-8 mg) were loaded into ceramic pans and were heated from room temperature to 800 °C at a constant heating rate of 10 °C /min. All runs were conducted under a nitrogen flow of 60 mL/min.

S1.3. Brunauer–Emmett–Teller (BET) surface area measurement, pore size analysis and contact angle measurement.

Micromeritics Gemini VI surface area and pore size analyser (Atlanta, GA, USA) was used to measure the Brunauer–Emmett–Teller (BET) surface area and analyse pore size and volume. This technique involves measuring volume of nitrogen gas adsorbed or desorbed at relative pressures ranging from 0.01 to 0.99.

The water contact angle of the electrospun systems was measured using the OneAttension optical tensiometer (Biolin Scientific, Espoo, Finland). Measurements were taken 4 s after depositing a 12 µl droplet of deionised water on the surface of each electrospun matte under ambient conditions.

S1.4. Modelling of drug release kinetics

Siponimod release kinetics from the drug-loaded implants were fitted to four different models to determine which model best describes the release behaviour in vitro. These models include the zero-order release, first-order release, and Higuchi models. Korsmeyer–Peppas model was not employed as the release percentage at the latest time point was below 60% of the loaded dose.

The zero-order release kinetics are explained by supplementary equation 1, where the fraction of drug released at time t (Q_t) is directly proportional to time (t). The slope of the

straight line is the zero-order release rate constant (K_0), and the intercept is the amount of the drug in the release medium at time zero equals (Q_0) (Supplementary Equation 1) [42,61].

$$Q_t = Q_0 + K_0.t$$ **(Supplementary Equation 1)**

For first-order release kinetics, the amount of released drug depends on the remaining concentration in the release system. It can be described by Supplementary Equation 2, where Qt represents the cumulative amount of drug release at the time "t", Q0 is the initial amount of the drug in the release medium at time zero, and K_1 is the first order release constant [42,43,61].

$$log\ Q_t = logQ_0 + \frac{(K_1.t)}{2.303}$$ **(Supplementary Equation 2)**

The Higuchi release model was developed to explain the drug release from insoluble matrices as a function of the square root of time. The model assumes that the initial drug concentration in the release system is higher than the drug solubility limit in the system, diffusion of the loaded drug from the matrix occurs in a single dimension, the rate of matrix body swelling, dissolution or degradation is negligible, drug distribution in and diffusivity from the matrix is constant and sink conditions are perfectly maintained at any time point.

The model is described by Supplementary Equation 3, where Q_t is the cumulative amount released at the time t and K_h is the Higuchi release constant [42,61].

$$Q_t = K_h.\ t^{1/2}$$ **(Supplementary Equation 3)**

S2. Supplementary results

S2.1. Effect of polymer concentration on electrospun products

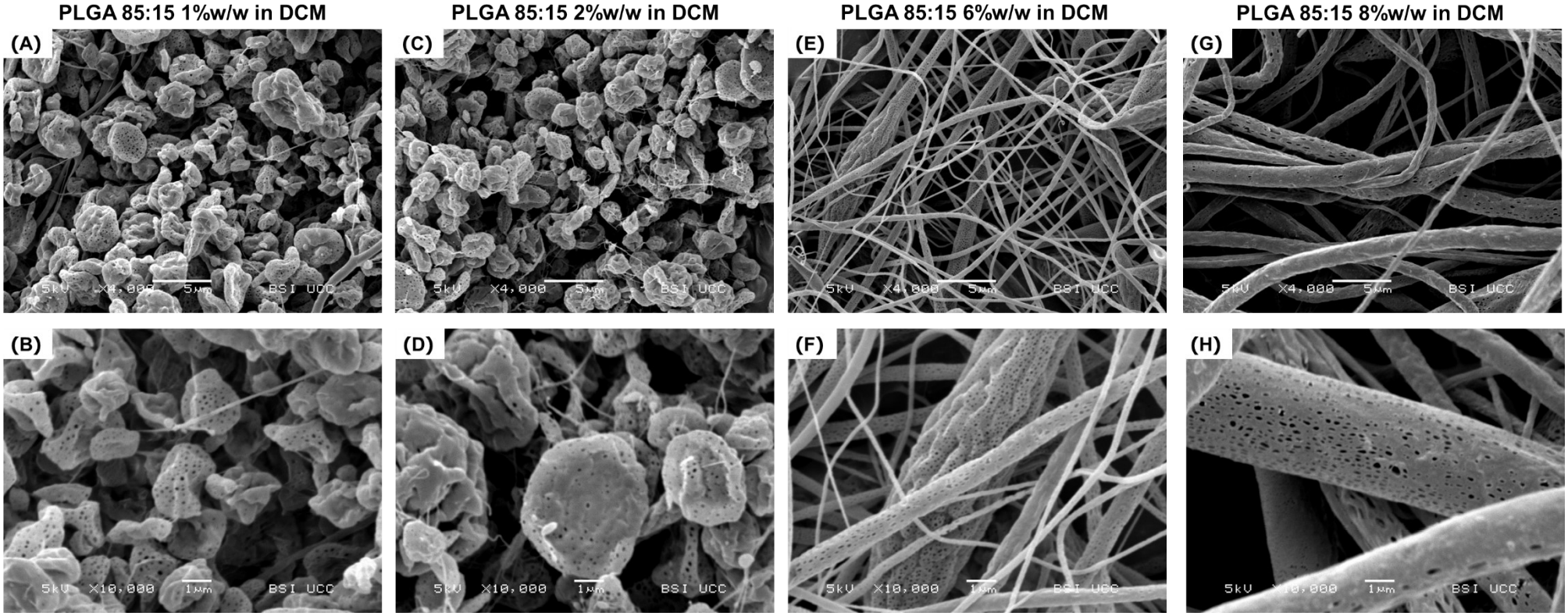

Fig. S1. Scanning electron micrographs of electrospun PLGA85:15 in increasing concentrations in dichloromethane (DCM). Electrospinning parameters were kept constant during the process. Electrospinning of successful fibres requires a minimum polymer concentration that results in sufficient polymer chain entanglement (entanglement concentration; C_e) [45,46]. Concentrations below C_e form beads as the jet breaks up into

small droplets, as seen in PLGA 1% w/w (panels A & B) and PLGA 2% w/w (panels C & D). Concentration $\geq C_e$ results in a sufficient entanglement causing fibre formation, as seen in PLGA 6% (panels E & F) w/w and PLGA 8% w/w (panels G & H). However, electrospinning of PLGA 6% w/w solution resulted in the formation of a beaded fibre, while electrospinning of the PLGA 8%w/w solution resulted in uniform, bead-free fibres. As the concentration of PLGA 85:15 increases from 6% w/w to 8%w/w, the mean fibre diameter increases from 0.38 ± 0.17 μm to 1.85 + 0.81 μm, respectively. All the electrospun PLGA 85:15 products, irrespective of polymer concentration, showed nano-pores covering the surface.

S2.2. Effect of solvent choice on electrospun products

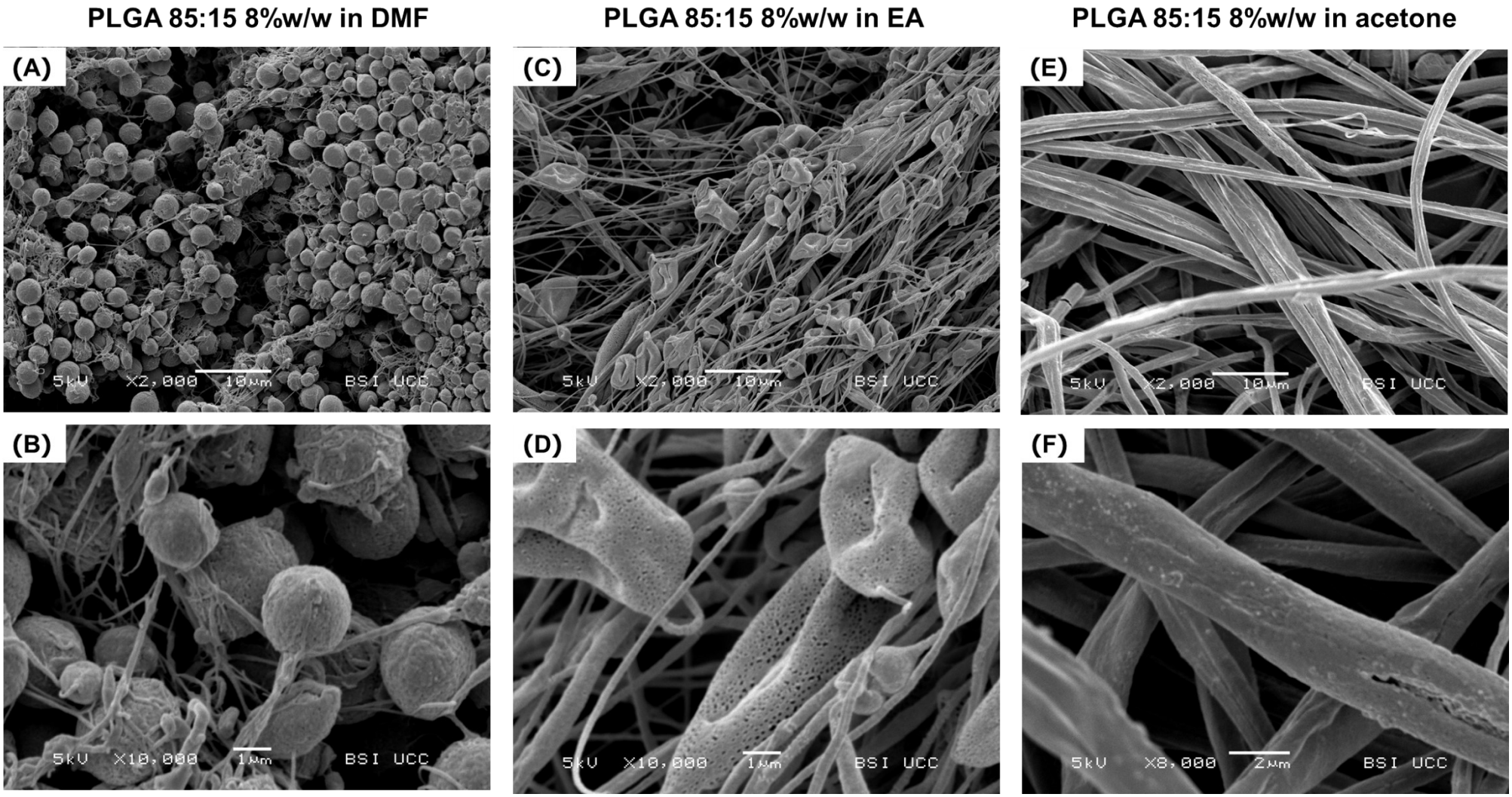

Fig. S2. Scanning electron micrographs of electrospun PLGA85:15 at a concentration of 8% w/w in different solvents, including dimethylformamide (DMF; panels A & B), ethyl acetate (EA; panels C & D) and acetone (panels E & F). Electrospinning conditions were kept constant in all experiments at a flow rate of 0.7 mL/h, voltage of 16 kV and collector distance of 15 cm from the emitter nozzle. Electrospinning of 8% w/w of PLGA 85:15 in DMF resulted in the formation of microparticles with a small fraction of thin interconnecting fibres (A & B), electrospinning of 8%w/w of PLGA 85:15 in EA resulted in the formation of a mixed population of large beads and thin fibres (C & D). The electrospinning of PLGA in acetone (E & F) resulted in the formation of uniform bead-free microfibres. Electrospun product from acetone is comparable to that from DCM at the same polymer concentration (Fig. S1 panels G & H), which also resulted in the formation of bead-free fibres. A summary of solvent properties used for electrospinning is summarised in Table S2. Considering the tested solvent properties, DMF exhibits the highest viscosity, suggesting that sufficient chain entanglement and a successful fibre formation process can be obtained by electrospinning PLGA at a lower concentration (< 8%) from DMF compared to other solvents. However, no fibres were obtained by electrospinning 8%w/w PLGA using DMF, while continuous bead-free fibres were successfully obtained by electrospinning PLGA at the same concentration from less viscous solvents (DCM and acetone). This can be explained by the significantly high volatility (reflected by high vapour pressure and low boiling point) of both DCM and acetone compared to the DMF. The high volatility rapidly increases the jet concentration during the flow towards the collector, achieving sufficient chain entanglement and successful electrospinning at a lower polymer concentration. This can explain why 8% w/w of PLGA in EA yielded a product of mixed fibres and beads compared to a bead-free fibre product using DCM. Ethyl acetate has comparable viscosity, dipole moment, and solubility parameters but significantly lower volatility than DCM (reflected by higher boiling point and lower vapour pressure). At

concentrations above the critical entanglement concentrations, the effect of viscosity can be observed in the difference between the fibre diameter of electrospun products from acetone and DCM. Acetone has a lower viscosity and higher boiling point than DCM, resulting in a slower solvent evaporation rate and lower viscoelasticity during electrospinning. Both facilitate the axial stretching of the jet and whipping into fibres with smaller diameters [46,52].

Solvent	**Viscosity at 25°C mPa.s**	**Dipole moment (Debye)**	**Dielectric constant at 20 °C**	**Solubility parameter ($cal^{1/2}$ $cm^{3/2}$)**	**Surface tension at 20°C (mN/m)**	**Boiling point (°C)**	**Vapour pressure at 21°C (mmHg)**	**Characteristics of the electrospinning product prepared using 8% w/w PLGA 85:15 solution in each solvent**
Acetone	0.33	2.9	20.60	10	23.3	56	194	Bead-free uniform microfibres with a mean diameter of 1.04 $\pm$ 0.35 μm*
Dichloromethane	0.45	1.8	9.1	9.7	28.1	40	376	Bead-free uniform microfibres with a mean diameter of 1.85 $\pm$ 0.81 μm*
Dimethyl-formamide	0.82	3.82	36.70	12.1	35.0	153	3.8	Mainly microparticles

Ethyl acetate	0.46	1.78	6.02	9.1	24	77	78	Mixed population of nanofibers and beads

Table S2. Physical and chemical properties of the solvents used in this study for optimisation of the electrospinning process, values were obtained from the Handbook of Organic Solvent Properties, Elsevier, 1996.

* Mean fibre diameter of 225 fibres ± standard deviation.

S2.3. Representative image of the electrospun microfibrous implant

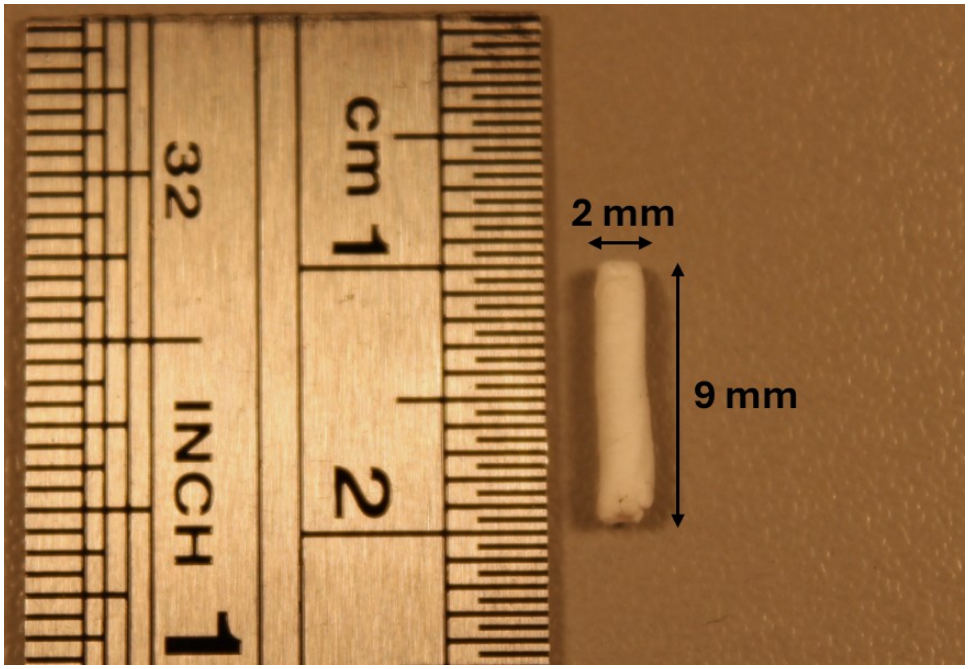

Fig. S3. Representative image of Si: PLGA (8:100) showing the implant dimensions. The implant was produced using the electrospinning conditions described in section 2.2.

S2.3. Surface area measurement, pore analysis and contact angle measurement of electrospun products

Table S3. The BET surface area, pore volume and pore size distribution analysis.

Formulation	BET surface area	Total pore volume	Average pore width*
ES PLGA	5.7836 m^2/g	0.042258 cm^3/g	292.2615 Å
Si:PLGA (12:100)	3.8883 m^2/g	0.006971 cm^3/g	71.7099 Å

* It is important to highlight that average pore width measurements are averages of total pores detected, including interfibres pores.

Table S4. Mean contact angle measurement.

Formulation	Mean contact angle [°]
ES PLGA	106.52 $\pm$ 3.97
Si:PLGA (12:100)	114.00 $\pm$ 19.98

The contact angle was recorded at 4 s $\pm$ 0.3 s. These values represent the average of three independent replicates (n=3), and in each replicate, the average of right and left contact angles was recorded.

S2.4. Effect of siponimod on the thermal decomposition of PLGA 85:15

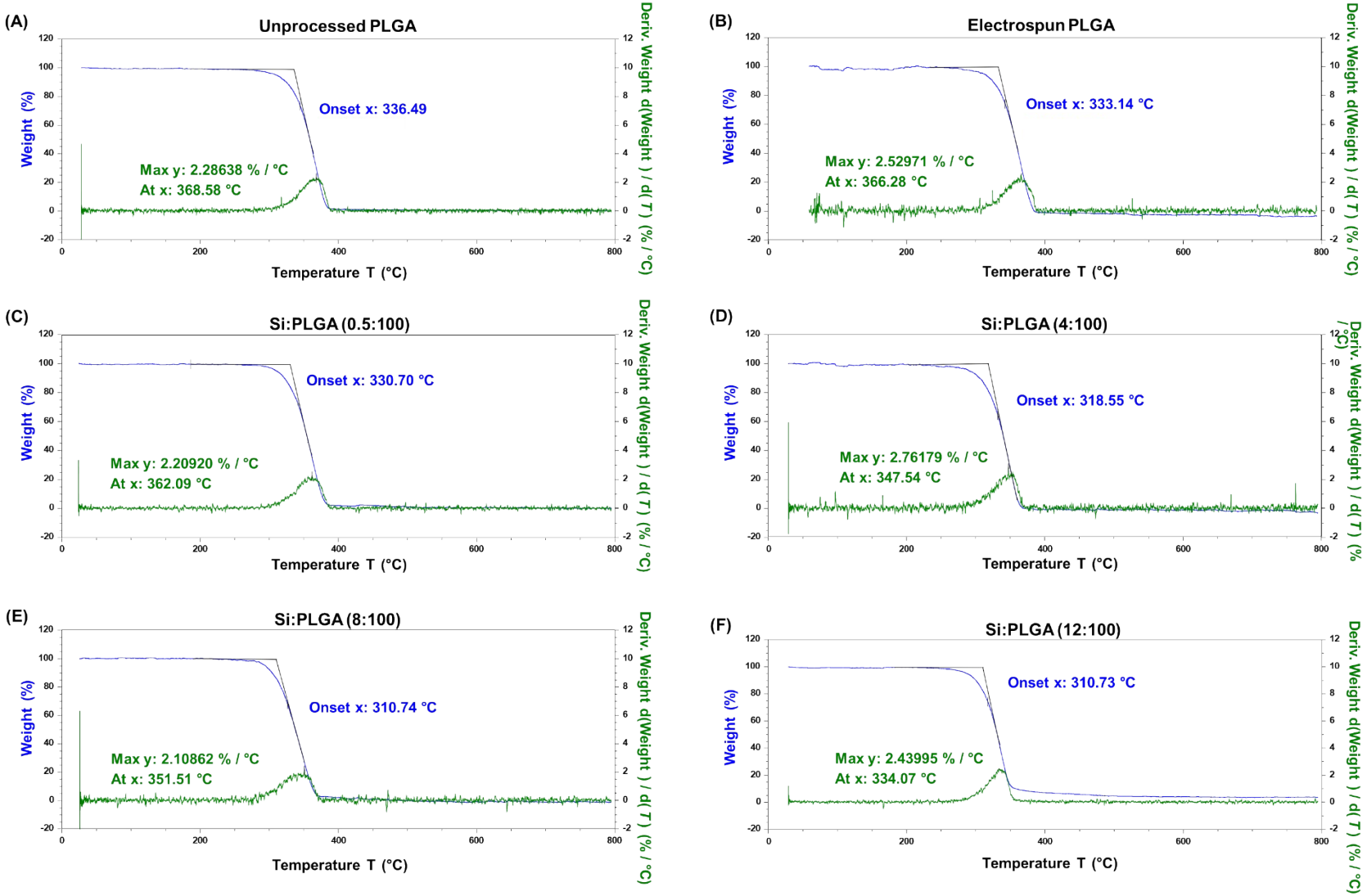

Fig. S4. Thermogravimetric analysis (TGA) of (A) unprocessed PLGA, (B) electrospun drug-free PLGA, (C) Si:PLGA (0.5:100), (D) Si:PLGA (4:100), (E) Si:PLGA (8:100) and (F) Si:PLGA (12:100). Onset X in each panel shows the decomposition extrapolated onset temperature, and Max Y shows the maximum decomposition rate at temperature X. Details of the formulation are presented in Table 1. Data handling was performed using the TRIOS 5.1.1. software (TA Instruments, New Castle, DE, United States).

S2.5. Distribution of siponimod in the electrospun fibres

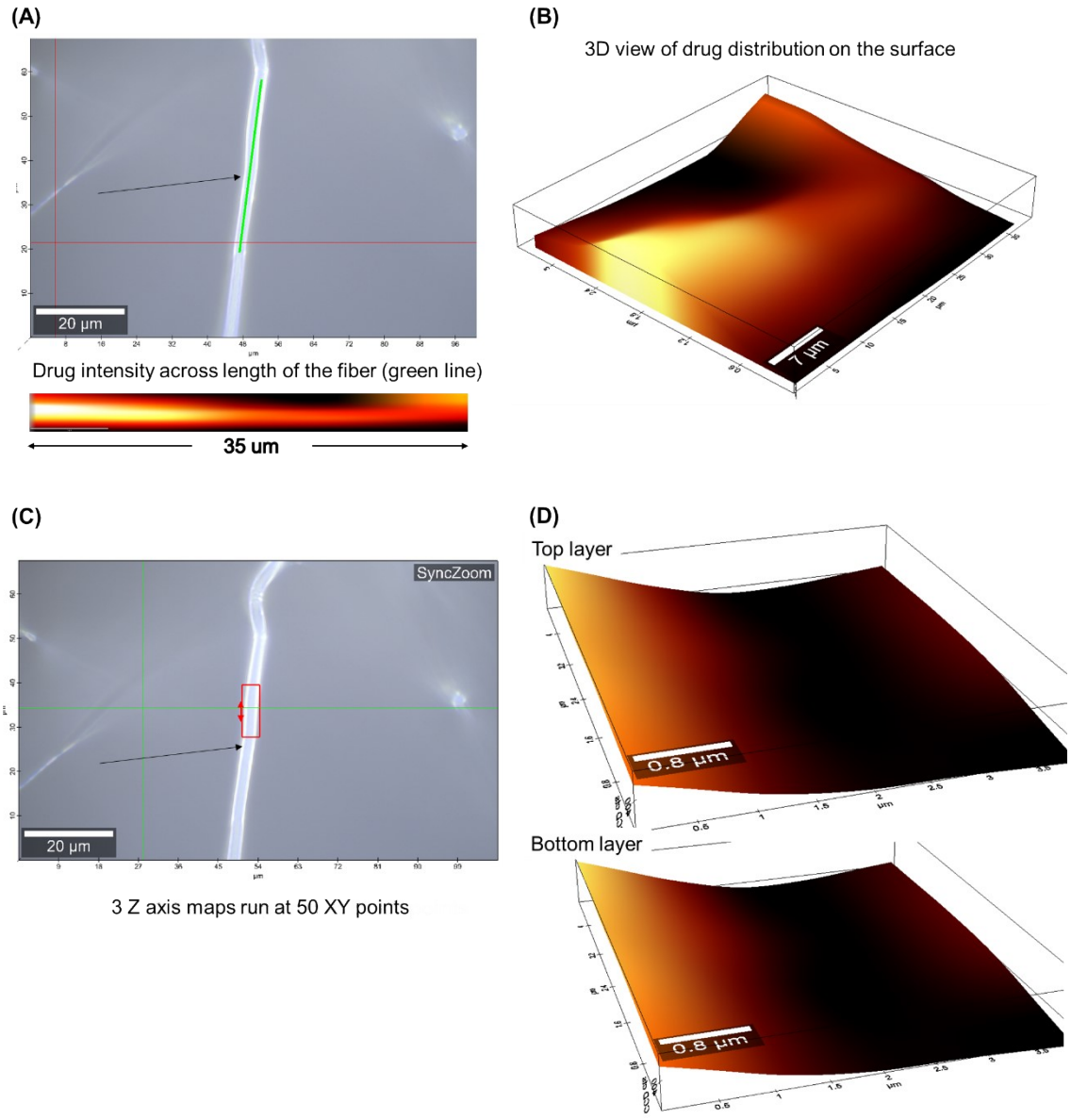

Fig. S5. (A) 3D maps were taken along the length of an individual microfibre (green line). XY maps were collected for 50 points for 35 µm length along the fibre, which was combined to form (B) a drug distribution map along the fibre's surface. (C) Individual XY maps were taken in a selected region (red box) at different Z depths to understand the drug distribution along the cross-section of the fibre. (D) The intensity plots show the Raman intensity obtained from the drug at the top (z=0) surface of the microfibre and bottom (z≈ 3.5 µm) of the microfibre (the bottom estimated refers to the point where the signal from the PLGA matrix is lost).

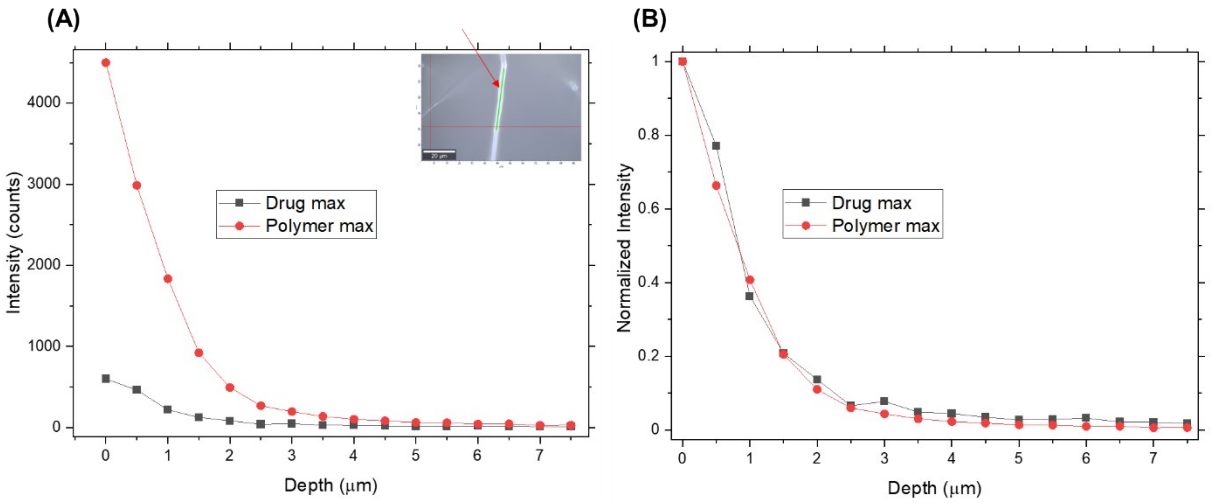

Fig. S6. Z map into the fibre depth showing siponimod distribution. Z maps were run on 50 individual points along the length of the fibre (green line) to understand the drug distribution in the cross-section of the fibre. The plots show the (A) absolute and (B) normalised intensities of Raman bands from the drug and the polymer at a single XY point. As observed, the drug intensities follow the same trend as the polymer, indicating the uniform drug presence along the depth of the fibre.